WATER RESOURCES RESEARCH, VOL. 37, NO. 12, PAGES 2965–2979, DECEMBER 2001

Pore-scale modeling of biological clogging due to aggregate expansion: A material mechanics approach

Hubert J. Dupin,[1] Peter K. Kitanidis, and Perry L. McCarty

Department of Civil and Environmental Engineering, Stanford University, Stanford, California, USA

Abstract. Whereas most previous studies of biomass growth and biological clogging consider continuous biofilms, we investigate how the growth of biomass in the form of aggregates affects the permeability and the transport properties of porous media. This paper presents modeling of processes in a single pore, and a companion paper [*Dupin et al*., this issue] describes modeling over a network of pores. Each pore (channel) is seeded with initial biomass that consumes an electron donor and an electron acceptor according to dual Monod kinetics. Biomass is modeled as a continuous uniform isotropic hyperelastic material, whose expansion and deformation are governed by material mechanics stress-strain relations, unlike traditional approaches that use ad hoc empirical schemes. The Stokes flow, the advection-diffusion-reaction mass transport, and the biomass deformation partial differential equations are solved using finite elements. The solute transport problem is made more computationally efficient by controlling the time step discretization. Results from a simulation illustrate the methodology.

1. Introduction

In situ bioremediation is a potentially cost-effective approach to clean up a polluted site. The essence of this approach is to use microorganisms to degrade pollutants in the ground. In some cases these pollutants serve as primary substrates, providing energy or carbon for the growth of the microorganisms. In other cases the pollutants are degraded by cometabolism; that is, the microorganisms grow on other substrates. In either case the microorganisms generally need some additional substrates and/or nutrients to sustain growth and degrade the pollutants. In natural attenuation, nutrients are already present. In enhanced bioremediation a feed solution is forced through the aquifer. These substrates and/or nutrients are generally provided in soluble form, and a chemical delivery and mixing scheme is usually critical for the success of enhanced in situ bioremediation. In general, the more substrate the microorganisms use, the greater the microbial population and the more the amount of the pollutant that can be degraded. However, as the mass of the microorganisms grows, the permeability of the formation tends to decrease, which restricts flow and the supply of substrates and/or nutrients [*McCarty et al*., 1998; *Rittmann*, 1993; *Taylor and Jaffe*, 1991; *Vandevivere and Baveye*, 1992b].

Biomass growth in porous media can occur in different morphologies [*Dupin and McCarty*, 2000]. The most commonly reported and modeled growth mode is through biofilms; that is, microorganisms grow as a continuous layer, the biofilm, on the surface of the soil grains [*Chen et al*., 1994; *Clement et al*., 1996; *Suchomel et al*., 1998; *Taylor and Jaffe*, 1990a, 1990b; *Taylor et al*., 1990]. Sometimes, however, the biomass does not cover the entire surface of the soil grains, and microcolonies (i.e., a patchy biofilm) develop [*Molz et al*., 1986]. In other cases, biomass grows in pores in the form of aggregates [*Vandevivere and Baveye*, 1992b] or a bioweb [*Paulsen et al*., 1997]. When fungal growth occurs, mycelia can develop throughout the entire pore volume and envelop several soil grains [*Dupin and McCarty*, 1999]. These forms of biomass growth can occur simultaneously [*Dupin and McCarty*, 2000]. For example, using the apparatus described by *Dupin and McCarty* [1999], seeding of silicon pore imaging elements and subsequent acetate feeding resulted in growth both of aggregates and of a continuous thin biofilm (Figure 1).

To distinguish between a continuous and a patchy biofilm, *Rittmann* [1993] proposed the use of the normalized surface loading or flux, which is the ratio of the actual substrate flux into the biomass to the minimum substrate flux that supports a steady state deep biofilm. From a review of published data he showed that at high values of this ratio a biofilm tends to be continuous, whereas at low values only patchy growth appears to be sustained. However, Rittmann recognized that this distinction is not crucial in modeling substrate consumption. *Baveye and Valocchi* [1989] showed that when the substrate concentration is uniform within the biomass entities and mass transfer is linear (i.e., proportional to the difference between the concentration within the bulk fluid and the concentration within biomass), both types of growth and substrate uptake could be modeled using similar equations, notwithstanding differences in the significance of the parameters.

Many models [*Clement et al*., 1996; *Cunningham et al*., 1991; *Suchomel et al*., 1998; *Taylor and Jaffe*, 1990b; *Taylor et al*., 1990] use porosity reduction as a critical parameter for assessing permeability reduction. Assuming a uniform coverage of the soil grains by biomass, porosity reduction is strongly correlated to permeability reduction as has been shown experimentally [*Cunningham et al*., 1991; *Taylor and Jaffe*, 1990a; *Vandevivere and Baveye*, 1992a, 1992b]. *Rittmann* [1993] noted that the difference between biofilm, microcolonies, or aggregate growth is crucial to model permeability reduction. It takes less biomass to plug a pore if it forms aggregates than if it

[1]Now at Geosciences Department, Exploration-Production Division, Gaz de France, Saint-Denis-La-Plaine, France.

Copyright 2001 by the American Geophysical Union.

Paper number 2001WR000306.
0043-1397/01/2001WR000306$09.00

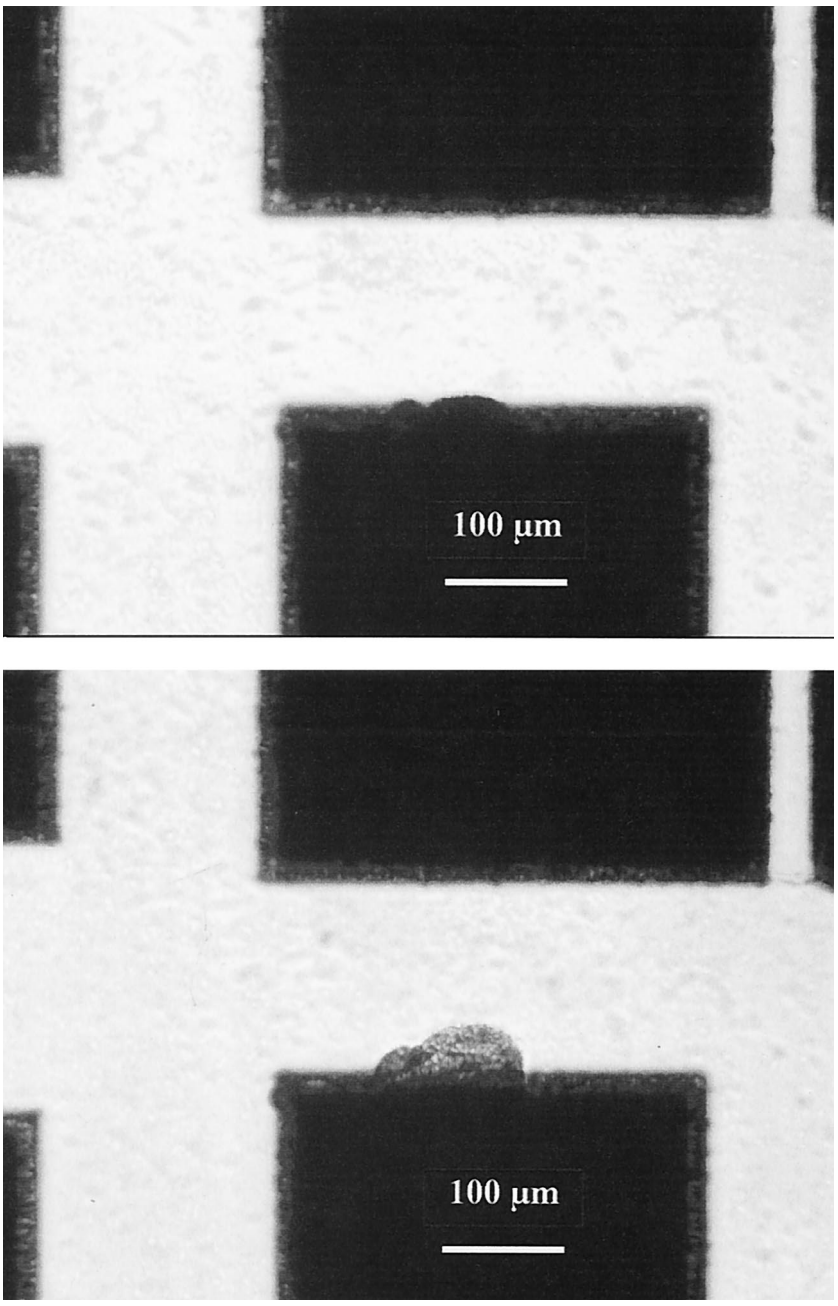

Figure 1. Growth of two aggregates observed in silicon pore imaging elements. In the micromodel, soil grains appear black, and texture in the pores corresponds to a thin biofilm. The bottom image was acquired 2 days after the top one.

forms a continuous biofilm. *Vandevivere et al*. [1995] showed that the assumption of a uniform coverage underestimates clogging in fine sands, whereas distributing biomass as plugs improved the predictions of the conductivity reduction.

Few authors have focused on modeling aggregate growth in porous media. *Chen et al*. [1996a] evaluated growth of aggregates in two-dimensional (2-D) channels. They validated their model using in situ dissolved oxygen sensor probes and an artificially constructed biofilm [*Cunningham et al*., 1995]. However, the numerical scheme of *Chen et al*. [1996a] did not allow the aggregates to grow to a thickness larger than 10–20% of the width of the channels. Thus they did not address permeability reduction.

Aggregate growth needs to be first represented adequately at the microscale before it can be upscaled. An appealing method consists in using network models, which have been used in percolation theory for >40 years [*Berkowitz and Ewing*, 1998; *Fatt*, 1956a, 1956b, 1956c]. Network models consist of an assemblage of channels (pores) that connect at nodes to interact with each other in a defined manner. Common applications of network models relate to the study of one-, two-, and three-phase flow. *Suchomel et al*. [1998] modeled biofilm growth and clogging in square and cubic lattice networks. *Dupin and McCarty* [2000] observed different biological growth morphologies in square lattice networks with random width.

This paper details the two-dimensional modeling of aggre-

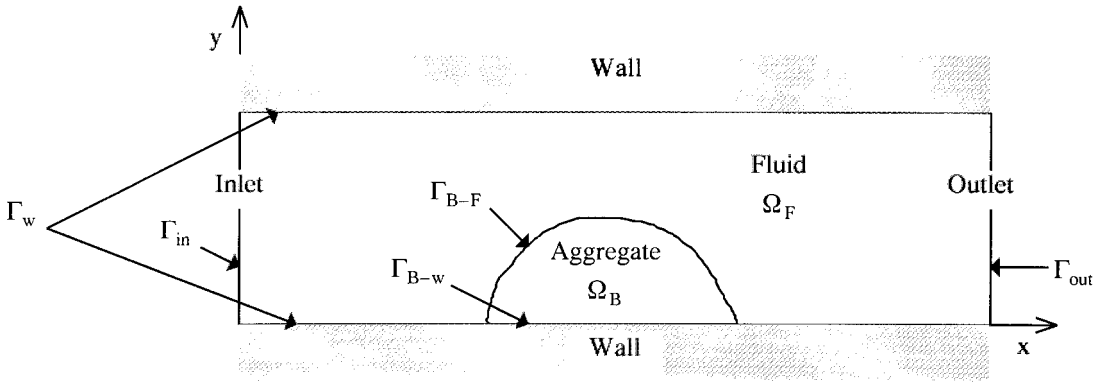

Figure 2. Schematic drawing of a pore.

gate growth and the effects of this growth on the permeability and the transport properties of a single pore. It presents results of a simulation as an illustration. A companion paper [*Dupin et al*., this issue] details how those pores are linked to form a network pore model idealizing a porous medium.

In our model, pores are seeded with initial biomass that consumes substrate and grows, reducing the permeability of the pores. Detachment is neglected in this work as aggregates in our experimental system have been observed to attach strongly to surfaces [*Dupin and McCarty*, 2000], and to simplify simulations, attachment of new aggregates is also neglected. The partial differential equations of flow and substrate transport are solved in the bulk fluid and in biomass aggregates using finite elements. Thus no empirical mass transfer boundary layer thickness is assumed, unlike many other biofilm models [*Chen et al*., 1994; *Williamson and McCarty*, 1976].

A crucial contribution of this work is a material-mechanics formulation to determine the aggregate expansion and deformation from the computed biomass. The flexibility of finite elements in representing complex and time-variant boundaries allows us to simulate the growth of aggregates and their filling of entire pore volumes, overcoming the difficulties encountered by *Chen et al*. [1996a], who used finite differences. Furthermore, aggregates can deform under the action of flow. However, in this paper the emphasis is on the effects of growth. We neglect the forces exerted by the fluid on the aggregates for the sake of computational efficiency, although we show how to account for them.

All variables vary with time but with different timescales. Flow transport has a typical relaxation time much less than a second, which means that a steady state condition is established almost instantaneously. Within a 600 μm long pore, substrate advective transport occurs with timescales of a few seconds, while substrate diffusion has a typical timescale of the order of minutes. Biomass growth is a much slower process, with a typical timescale of hours. Thus we can treat the flow, the substrate transport, and the biomass growth sequentially, as done in many other biofilm models [*Rittmann and McCarty*, 1981]. For example, when solving for advection, diffusion, and consumption of substrate within a pore, we can consider the flow to be instantaneously equilibrated, while biomass growth appears almost frozen.

We will first detail the equations governing the behavior of a single pore. Then, we will show how those equations were implemented numerically. Finally, we will present preliminary results of a simulation. *Dupin et al*. [this issue] show the influence of the parameters on the overall clogging potential of the simulated porous media, idealized as a network model.

2. Description of the Pore Model

In this section we present the equations governing the modeled phenomena thought to control aggregate growth: fluid flow, substrate transport, substrate consumption in the aggregates, and biomass deformation. For all purposes, biomass aggregates are considered continuous, homogeneous, and isotropic. The model is two-dimensional. The x axis is along the axis of the pore, the origin being the initial center of the aggregate; the y axis is across the pore, the origin being the plane of attachment of the aggregate. Figure 2 shows the geometry of one pore, the different domains, and the boundaries.

2.1. Fluid Movement

In each pore, fluid flows according to Stokes equations (i.e., creeping flow). The velocity $\mathbf{u} = (u_x, u_y)$ and the pressure expressed as hydraulic head θ are governed by the following equations, where $\nu_{S_{\text{eff}}}$ is the effective kinematic viscosity and g is the gravity:

$$\begin{aligned} \frac{\nu_{S_{\text{eff}}}}{g}\left(\frac{\partial^2 u_x}{\partial x^2}+\frac{\partial^2 u_x}{\partial y^2}\right)-\frac{\partial \varphi}{\partial x}=0 \\ \frac{\nu_{S_{\text{eff}}}}{g}\left(\frac{\partial^2 u_y}{\partial x^2}+\frac{\partial^2 u_y}{\partial y^2}\right)-\frac{\partial \varphi}{\partial y}=0 \end{aligned} \tag{1}$$

in $\Omega = \Omega_B \cup \Omega_F$ and

$$\nabla \cdot \mathbf{u} = 0 \tag{2}$$

in $\Omega = \Omega_B \cup \Omega_F$. The boundary conditions are given on Γ_{in} by the prescribed parabolic profile for u_x and

$$u_y = 0 \tag{3}$$

and on Γ_{out} is given by

$$\begin{aligned} \frac{\partial \mathbf{u}}{\partial x} = 0 \\ \int_{\Gamma_{\text{out}}} \varphi dA = 0 \end{aligned} \tag{4}$$

Table 1. Parameters of the Model

Parameter	Value	Signification
Dimensions		
L_{pore}	600 μm	length of each pore
W_{pore}	typically 100 μm	width of each pore
$R_{\text{aggregate}_0}$	5 μm	size of the initial seed
	20°C	temperature
Biological kinetics		
K_{sA}	1.0 mg L^{-1}	saturation constant for oxygen
K_{sD}	1.0 mg L^{-1}	saturation constant for phenol
k	9.3 mg mg^{-1} d^{-1}[a]	maximum utilization rate
Y	0.61 mg mg^{-1}[a]	yield coefficient
b	0.12 day^{-1}[a]	decay coefficient
f_d	0.8 mg mg^{-1}[b]	degradable biomass fraction
d_c	1.42 mg mg^{-1}[b]	decay oxygen demand
COD	2.38 mg mg^{-1}[b]	chemical oxygen demand of phenol
$F = \text{COD} - Yd_c$	1.52 mg mg^{-1}[b]	oxygen to phenol utilization ratio
X_m	30,000 mg L^{-1}[b]	maximum solids concentration in aggregate
$X_{a\,\text{Start}}$	$X_m 1$	initial active biomass concentration ($f_a = 1$)
Hydrodynamics		
D_a	2.32 cm^2 d^{-1}[c]	aqueous oxygen diffusion coefficient
D_{fa}	1.85 cm^2 d^{-1}[c]	oxygen diffusion coefficient in aggregate
D_d	1.01 cm^2 d^{-1}[c]	aqueous phenol diffusion coefficient
D_{fd}	0.81 cm^2 d^{-1}[c]	phenol diffusion coefficient in aggregate
g	9.81 m s^{-2}	gravity
ρ	998 mg cm^{-3}[d]	density of water
υ_{water}	0.01003 cm^2 s^{-1}[d]	kinematic viscosity of water
λ	2.10^3	relative viscosity of water in aggregate
Mechanics		
μ_L	0.01 MPa	lame coefficient
	16.7°	minimum angle of contact
	2 μm	minimum distance before contact
Iterations		
Δt	12 min	time step to update shape of biomass

[a]Source is *Shurtliff et al*. [1996].
[b]Source is *Dupin* [1999].
[c]Values are estimated using the method of *Hayduk and Laudie* [1974] as reported by *Dupin* [1999] and *Montgomery* [1996].
[d]Source is *Lide* [1991, p. 6.8].

and on $\Gamma_w \cup \Gamma_{B-w}$ is given by

$$\mathbf{u} = 0. \tag{5}$$

In this subproblem we are interested in computing the head loss, which is the difference between the head at the inflow and the outflow boundaries. At the outlet the mean of φ is set arbitrarily to zero. The solution yields the head loss for the prescribed pore inlet velocity so that the conductance can be computed.

A pseudoviscosity for flow within the aggregate was set much higher than the normal water viscosity to account for increased resistance. Hence $\nu_{S_{\text{eff}}} = \lambda \nu_{\text{water}}$ in the aggregate, where $\lambda = 2000$. Such a high coefficient can induce pore and network permeability reductions by a factor of 2000 if biomass completely fills the pores, consistent with the limit on permeability reduction reported by *Taylor and Jaffe* [1990a].

Because φ is set to zero, on average, on the outlet boundary, the pressure drop across the pore is obtained by

$$\Delta\varphi = \frac{\int_{\Gamma_{\text{in}}} \varphi \, d\Gamma}{\Gamma_{\text{in}}}. \tag{6}$$

The (pore) hydraulic conductivity, which will be reported by *Dupin et al*. [this issue], is defined as the ratio of the discharge through the pore u_{ave} to the average gradient of head across the pore, $(u_{\text{ave}} L_{\text{pore}})/\Delta\varphi$, with units of $[L\ T^{-1}]$.

2.2. Advection and Diffusion

The substrates, electron acceptor (oxygen) and electron donor (phenol), with respective concentrations C_A and C_D, undergo advection and diffusion throughout the entire pore volume. They are consumed in the biomass Ω_B according to dual Monod kinetics: The electron acceptor is used for cell growth and decay, while the electron donor is utilized only for cell growth. We distinguish between active biomass, X_A, and inert remains, X_I. In the bulk domain Ω_F (fluid), there is no biomass, $X_A = 0$ and $X_I = 0$, hence there is no substrate consumption. The effective diffusion coefficient D_{eff}, is lower in the aggregate than in the bulk fluid. *Williamson and McCarty* [1976] recommend using a value 80% of the diffusion coefficient in the aqueous phase.

The model can be expressed by the equations presented by *Semprini and McCarty* [1991]. The parameters are explained in Table 1. Because the concentrations of electron donor (phenol) and electron acceptor (oxygen) get involved only through

the ratio C/K_S, the saturation constants K_S have been set to 1 mg L^{-1} to simplify the comparisons between concentrations of electron donor and electron acceptor. This simplification is practically equivalent to making each concentration dimensionless by dividing by its saturation constant. A term for decay under anaerobic conditions could eventually be added in (9) and (10), but such decay would proceed at a much slower rate than decay under aerobic conditions. Oxygen is assumed in our simulations to be always present; thus the model as formulated describes decay sufficiently well. We have in Ω for (7) and (8)

$$\frac{\partial C_A}{\partial t} - D_{A_{\text{eff}}}\nabla^2 C_A + \mathbf{u}\cdot\nabla C_A = -X_A \frac{C_A}{C_A + K_{S_A}} \cdot \left(kF \frac{C_D}{C_D + K_{S_D}} + d_f d_a b \right) = F_1(X_A, C_A, C_D), \tag{7}$$

$$\frac{\partial C_D}{\partial t} - D_{D_{\text{eff}}}\nabla^2 C_D + \mathbf{u}\cdot\nabla C_D = -kX_A \frac{C_A}{C_A + K_{S_A}} \frac{C_D}{C_D + K_{S_D}} = F_2(X_A, C_A, C_D) \tag{8}$$

and in Ω_B for (9) and (10)

$$\frac{\partial X_A}{\partial t} = X_A \frac{C_A}{C_A + K_{S_A}} \left(kY \frac{C_D}{C_D + K_{S_D}} - b \right) = F_3(X_A, C_A, C_D) \tag{9}$$

$$\frac{\partial X_I}{\partial t} = X_A \frac{C_A}{C_A + K_{S_A}} b(1 - f_d) = F_4(X_A, C_A). \tag{10}$$

We have $F_1 = 0$ and $F_2 = 0$ in Ω_F as $X_A = 0$ there. The boundary conditions are a constant supply on Γ_{in}

$$\begin{aligned} u_{\text{ave}} C_A - D_A \frac{\partial C_A}{\partial x} &= u_{\text{ave}} C_{A_{\text{supply}}} \\ u_{\text{ave}} C_D - D_D \frac{\partial C_D}{\partial x} &= u_{\text{ave}} C_{D_{\text{supply}}}, \end{aligned} \tag{11}$$

no diffusion gradient on Γ_{out}

$$\begin{aligned} \frac{\partial C_A}{\partial x} &= 0 \\ \frac{\partial C_D}{\partial x} &= 0, \end{aligned} \tag{12}$$

and no flux through $\Gamma_w \cup \Gamma_{B-w}$ (wall).

$$\begin{aligned} \frac{\partial C_A}{\partial y} &= 0 \\ \frac{\partial C_D}{\partial y} &= 0. \end{aligned} \tag{13}$$

The essence of (12) is that mass flux in the channel is not affected by the value of concentration at its downgradient end, as will be explained by *Dupin et al.* [this issue]. This assumption is valid for a sufficiently long channel. At $t = 0$, $C = C_{\text{supply}}$ for the electron donor and the electron acceptor throughout the entire pore.

2.3. Biomass Deformation

2.3.1. Physical description. Several authors have modeled biomass growth in terms of aggregates. In a recent approach using a discrete cellular automaton, *Picioreanu et al.* [1998b] considered that following its growth within an aggregate, a cell expands and randomly pushes its surrounding cells. This is achieved numerically by discretizing the space occupied by the biomass into boxes. Once the density in one of these boxes becomes greater than a maximum value at the end of a time step, half of the mass of that box stays in place and half overflows into a randomly chosen adjacent box (empty if possible, already occupied otherwise). They iterate this process for all the boxes that need to overflow during that time step. Thus this process in time increases the size of the aggregate as biomass eventually overflows into the empty boxes at the periphery of the aggregate. Picioreanu et al. did not take into account the energy necessary to push those surrounding cells. Although they claimed their deformation behavior is purely dictated by local rules (interaction with the immediate surrounding cells), they, in fact, neglected the sum of the individual contributions of each expanding cell mechanism to the total potential energy. In this paper, we consider that an aggregate expands and deforms by minimizing the energy required for that deformation. We base our assumption on the resistance the whole extracellular polymer matrix surrounding the cells might create during that deformation. Furthermore, if external forces are applied on an aggregate, the additional deformation is such that it minimizes the potential energy.

On the basis of our experiments (H. Dupin and P. L. McCarty, unpublished data, 1999), aggregates appear to behave as "elastic" solids, bending with the flow and regaining their original position when the flow is stopped. Thus we model the biomass body as elastic. Because the deformation of an aggregate can be extreme (growth can lead to an expansion by a factor of up to 2000 after a period of a couple of days), the stress-strain relation cannot be linear. The concept of hyperelasticity comprises two assumptions: The strain may be large, and the mechanical stresses within the aggregate depend solely on the aggregate initial and final positions and not the particular path in between. The latter assumption means that there is a strain energy function, which is determined by the present state of deformation only. In particular, this assumption excludes plasticity and viscoelasticity. The neo-Hookean hyperelasticity, which is a generalization of elasticity for large deformations [*Bonet and Wood*, 1997], is one of the simplest nonlinear stress-strain expressions and reduces under small deformations to the commonly used linear stress-strain expressions. Mathematical formulations will be detailed in section 2.3.2.

We also assume that the biomass body is incompressible in a purely mechanical sense; that is, it does not shrink or expand under pressure, maintaining a constant density. The biomass growth or decay would result in an expansion or contraction of aggregate volume, so that the biomass density is maintained constant. This might be a simplification of reality. However, a biofilm or aggregates are generally modeled as having an average constant density [*Anderson*, 1996; *Rittmann and McCarty*, 1980]. Because true incompressibility is difficult to enforce with finite element methods without inducing artificial stiffening or locking [*Bonet and Wood*, 1997], pseudo-incompressibility in a purely mechanical sense is used: It is analogous to using a finite but very large bulk modulus.

A typical hyperelastic isotropic incompressible neo-Hookean material is rubber. Under isothermal conditions, rubber is hyperelastic and incompressible. Nevertheless, it undergoes thermal expansion [*Nicholson and Lin*, 1996].

As the domain is 2-D, as depicted in Figure 2, the aggregates undergo plane strain: Deformation in the third dimension (depth) is prevented so that displacements are only allowed in the plane x-y.

2.3.2. Mathematical formulation. Define $\mathbf{X}$ as the original (material) coordinate of a point at $t = 0$, $\boldsymbol{\phi}(\mathbf{X}, t)$ as the position of the biomass body at time t, $\mathbf{F} = \partial\boldsymbol{\phi}/\partial\mathbf{X}$ as the deformation gradient, $\mathbf{C} = \mathbf{F}^T\mathbf{F}$ as the right Cauchy-Green deformation tensor, and $J = \det(\mathbf{F})$ as the Jacobian of $\mathbf{F}$. Thus $J^2 = \det(\mathbf{C})$. The total deformation can be expressed as the combination of two artificial deformations. The first one describes the isochoric or distortional deformation during which the material does not expand but is distorted. The second one is an isotropic expansion. Mathematically, this is described as

$$\mathbf{C} = J^{2/3}\hat{\mathbf{C}}. \tag{14}$$

$\hat{\mathbf{C}}$ is called the deviatoric part of $\mathbf{C}$ ($\det \hat{\mathbf{C}} = 1$), and $J^{2/3}$ represents the isotropic expansion as the material is inherently three-dimensional.

Hyperelastic materials can be described by a stored energy function or elastic potential Ψ per unit undeformed volume. The condition that this hyperelastic potential Ψ depends only on the initial and the final configurations is expressed as

$$\Psi = \Psi(\mathbf{C}). \tag{15}$$

The potential of a neo-Hookean pseudoincompressible material is sometimes expressed as the sum of two terms [*Bonet and Wood*, 1997]. The first one depends on the deviatoric part of the deformation; the second one depends on the expansion and the deviation from the strict incompressibility. Thus

$$\Psi(\mathbf{C}) = \hat{\Psi}(\mathbf{C}) + U(J), \tag{16}$$

where

$$\hat{\Psi}(\mathbf{C}) = \Psi(\hat{\mathbf{C}}) = \frac{\mu_L}{2}(\operatorname{tr}\hat{\mathbf{C}} - 3) \tag{17}$$

and μ_L is the Lame coefficient. In the context of thermohyperelasticity, *Nicholson and Lin* [1996] proposed

$$U(J) = \frac{\kappa}{2}\left\{\frac{J}{[1 + \alpha(T - T_0)]^3} - 1\right\}^2, \tag{18}$$

where α is the volumetric thermal expansion coefficient, κ is the isothermal bulk modulus, and T is the temperature. For pseudoincompressible materials, κ takes high values and J tends to $[1 + \alpha(T - T_0)]^3$. By analogy, we propose

$$U(J) = \frac{\kappa}{2}\left(\frac{J}{\theta} - 1\right)^2, \tag{19}$$

where θ is the total expansion of a point in the aggregate since $t = 0$. Here θ represents the ratio of mass of all the daughter cells of an ancestor cell to the mass of that ancestor cell.

The total potential energy of the biomass aggregate $\Pi_L(\boldsymbol{\phi})$ can be expressed as

$$\Pi_L(\boldsymbol{\phi}) = \int_{\Omega_{B_0}} \Psi(\mathbf{C})\, dV - \int_{\Omega_{B_0}} \mathbf{f}_0 \cdot \boldsymbol{\phi}\, dV - \int_{\Gamma_{B-F}\cup\Gamma_{B-w}} \mathbf{t}_0 \cdot \boldsymbol{\phi}\, da, \tag{20}$$

where Ω_{B_0} is the initial biomass domain, $\mathbf{f}_0$ are the body forces, and $\mathbf{t}_0$ are the traction forces on the actual boundary. Note that the third term in the right-hand side is actually integrated only where the displacement $\boldsymbol{\phi}$ is not prescribed. Body forces due to densimetric differences (difference of weight and buoyancy) are neglected as cells have a density close to that of water and fluid forces would likely be much larger than such body forces.

To find the current state of deformation $\boldsymbol{\phi}$, we need to minimize $\Pi_L(\boldsymbol{\phi})$. However, this formulation cannot be easily implemented in a finite element scheme. We need, instead, to introduce an additional variable P as a Lagrange multiplier that can be recognized as the internal pressure (opposite of the hydrostatic pressure). Thus (16) is replaced by

$$\Psi = \Psi(\mathbf{C}, P) = \hat{\Psi}(\mathbf{C}) + P(J - \theta). \tag{21}$$

Such a modification is common in the finite element treatment of isothermal pseudoincompressible materials [*Bonet and Wood*, 1997]. The total potential energy of the biomass aggregate can then be expressed as

$$\Pi_L(\boldsymbol{\phi}) = \int_{\Omega_{B_0}} \hat{\Psi}(\mathbf{C})\, dV - \int_{\Omega_{B_0}} P(J - \theta)\, dV - \int_{\Gamma_{B-F}\cup\Gamma_{B-w}} \mathbf{t}_0 \cdot \boldsymbol{\phi}\, da. \tag{22}$$

The term

$$\int_{\Omega_{B_0}} P(J - \theta)\, dV$$

represents the Lagrange multiplier contribution necessary to enforce both the expansion due to growth and the incompressibility in a pure mechanical sense. The directional derivative of Π_L with respect to P in the arbitrary direction δp is

$$D\Pi_L(\boldsymbol{\phi}, P)[\delta p] = \int_{\Omega_{B_0}} \delta p(J - \theta)\, dV. \tag{23}$$

At equilibrium, $\forall\ \delta p$,

$$D\Pi_L(\boldsymbol{\phi}, P)[\delta p] = 0, \tag{24}$$

thus enforcing $J = \theta$.

2.3.3. Boundary conditions. Because the emphasis in this paper is on the effects of biological growth, we neglect for the sake of simplicity the forces exerted by the fluid on the aggregates compared to the internal forces arising from the deformation due to growth. Nonetheless, it is possible to account for the fluid forces as shown in section 2.3.2.

We require that each aggregate can move along each of its surfaces of contact with a wall (Γ_{B-w}) with no frictional resistance and no detachment while the middle point on each of these surfaces is kept fixed. This scheme preserves the general shape of the aggregates until they become substrate limited (when growth occurs mainly on their upgradient portion) or they become squeezed by the opposite wall. This is consistent with aggregate growth observed by H. Dupin and P. J. McCarty (unpublished data, 1999) and shown in Figure 1.

We impose two additional auxiliary conditions to enhance the numerical stability of the model, accelerate convergence, and simplify meshing. The minimum tangent of contact is arbitrarily set to 0.3 (minimum angle 17°). This is equivalent to setting a maximum surface tension at the biofilm-wall inter-

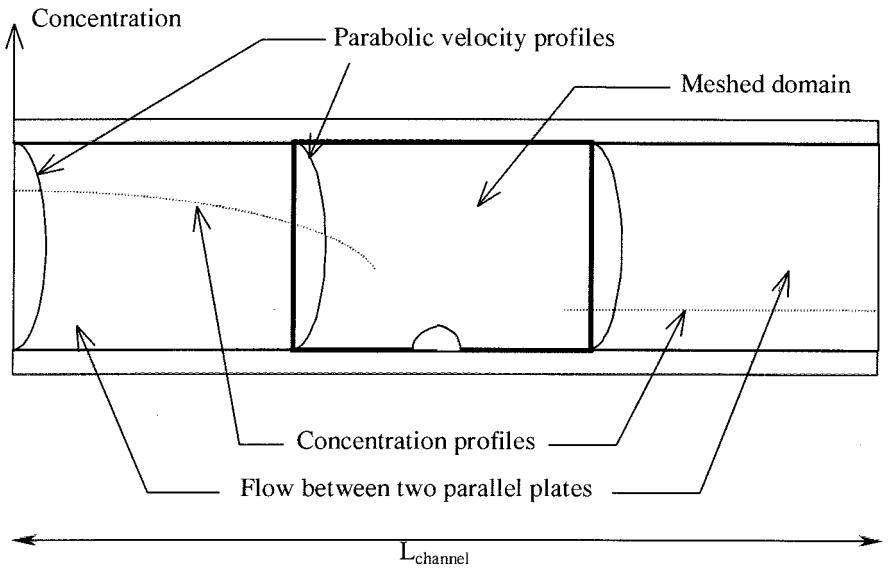

Figure 3. Illustration of boundary conditions for the meshed domain and the full pore.

face. Additionally, if the aggregate is separated from an opposing wall by a layer of fluid thinner than 2 μm, then contact of the aggregate to that wall is enforced (closing the pore). These two boundary conditions (minimum angle and minimum distance) appear reasonable.

If the fluid forces acting on aggregates were significant compared to the internal forces arising from growth, fluid would act on Γ_{B-F} as a normal force (pressure) and a tangential force (shear). These forces would be computed from the solution of the Stokes problem. However, accounting for them would require iterations as a new shape of the aggregate would lead to a new fluid velocity field and new forces acting on the aggregate boundary. This is likely to result in lengthy computations, deemed unnecessary at this point.

If microorganisms are tightly bound to the surface, tangential forces appear along the surfaces of contact of the aggregate with a wall, with the effect of preventing extension of the aggregate along these surfaces. Such boundary conditions would lead to highly distorted aggregate geometry. Similarly, if fluid forces can deform the aggregates, the resulting geometry might be very distorted. Finite element methods would not perform well because of the successive remeshing needed to keep a triangulation of an acceptable quality and the consequent loss of information, whose cumulative effect could be significant. One would need to use meshless methods, such as the reproducing kernel particle method [*Chen et al.*, 1996b], but at a significantly higher computational cost.

3. Numerical Implementation

The Stokes flow, substrate transport, and biomass deformation problems are all solved using Galerkin finite element formulations. We used a single mesh with linear triangular elements for all the different variables. The numerical model has been written using Matlab 5.1 for Sun WorkStation (see The MathWorks Inc. at www.mathworks.com), and routines for meshing and solving linear systems of equations come from that software.

3.1. Space Discretization

Numerical experiments suggest that it is unnecessary to discretize pores over their full lengths. In particular, away from an aggregate, flow is the same as between two parallel plates (parabolic velocity profile and linear change in the hydraulic head). Isoconcentration lines are perpendicular to the main pore axis, and concentration gradients change exponentially with distance from the inlet (as in a one-dimensional channel subject to steady state advection and dispersion with no sink). Such an advection-dispersion problem is described by

$$D_{\text{eff}} \frac{\partial^2 C}{\partial x^2} = u_{\text{ave}} \frac{\partial C}{\partial x}, \tag{25}$$

where D is the dispersion coefficient. With the boundary condition given by (11), the solution of this differential equation can be written as

$$C(x) = C_{\text{supply}}\left[1 - \alpha \exp\left(\frac{u_{\text{ave}} x}{D_{\text{eff}}} \right) \right], \tag{26}$$

where x is the abscissa along the pore (the origin being at the center of the initial aggregate) and α is function of the substrate consumption in the biomass.

Therefore it is advantageous to mesh only the central portion of each pore (Figure 3). The boundary conditions that we presented in section 2 for the inlet and outlet boundaries of each pore are also valid at the edges of the meshed domain. In particular, the inlet and outlet boundary conditions of the advection-diffusion problem are preserved as they represent continuity of substrate supply (mass flux).

If W_{pore} is the pore width and $R_{\text{aggregate}}$ is the aggregate maximum thickness, numerical experiments showed that we need to discretize the pore over its entire width and up to a distance $5R_{\text{aggregate}}$ or $1W_{\text{pore}}$ from the aggregate, whichever was the smaller, both in the upstream and downstream directions. To allow for expansion of the aggregate without having to extend the computational domain at each iteration, the mesh is initially generated up to a distance from the aggregate

which is the smaller of $10R_{\text{aggregate}}$ or $1.5W_{\text{pore}}$, both in the upstream and downstream directions. When, as a consequence of growth, the aggregate comes closer to the upstream or downstream edge of the meshed domain than $7R_{\text{aggregate}}$ or $1.3W_{\text{pore}}$, the meshed domain is extended to fit the meshing criteria. The adjustments continue until the full pore domain is entirely meshed.

3.2. Stokes Flow

Stokes flow is solved using a mixed formulation (velocity and pressure), using an elementwise stabilization term added to the mass conservation equation (2) [*Cao*, 1995; *Hughes and Franca*, 1987]. Element stiffness matrices and right-hand side vectors are given by *Dupin* [1999], following [*Cao*, 1995].

3.3. Advection and Diffusion

3.3.1. Principle of temporal discretization. We solve the partial differential equations (7)–(10) as did *Cao and Kitanidis* [1998], using a predictor-corrector modified Gear scheme. Boundary conditions were incorporated into the Galerkin formulation. Through this method the partial coupled differential equations are both decoupled and linearized. Element stiffness matrices and right-hand side vectors are given by *Cao and Kitanidis* [1998] and *Dupin* [1999].

3.3.2. Optimization of the temporal discretization. The above-mentioned scheme is a priori not stable for long time steps. However, the only deviation from steady state results from microorganism growth with a typical time scale of hours. Thus we use the amplitude of the difference within the aggregate between the concentration values of the prediction and correction substeps to control the numerical scheme. This criterion leads to initial time steps of a few minutes down to time steps of the order of a second, while keeping the results accurate to within 0.1%.

Because biomass expansion is carried out periodically and not continuously, the concentration profiles need to be updated to be consistent with the new biomass distribution after each aggregate expansion. Toward this need, the time discretization scheme is started and iterated, computing the biomass uptake F_1 and F_2 in (7) and (8) but by arbitrarily setting $F_3 = F_4 = 0$ in (9) and (10) until the concentration profiles no longer change, at which point these profiles are consistent with the biomass distribution. The normal temporal discretization scheme is then iterated.

3.4. Biomass Deformation

Cell growth temporarily results in an increase in biomass density without expansion. Then, every $\Delta t = 12$ min, the aggregate is deformed to bring the density back to the required density.

We use a mixed formulation problem, the displacements and the internal pressure being linearly interpolated. The resulting system of nonlinear equations was linearized and solved using a Newton-Raphson scheme as detailed by *Bonet and Wood* [1997]. To render the resulting linearized system matrix nonsingular and avoid artificial stiffening, an elementwise stabilization term is added to (22), analogous to the one used for solving the Stokes flow problem (T. J. R. Hughes, personal communication, 1998), so that (22) becomes

$$\Pi_L(\boldsymbol{\phi}, P) = \int_{\Omega_{B_0}} \hat{\Psi}(\mathbf{C})\, dV + \int_{\Omega_{B_0}} P(J-\theta)\, dV - \int_{\Gamma_{B-w}\cup\Gamma_{B-F}} \mathbf{t}_0 \cdot \boldsymbol{\phi}\, da + \frac{1}{2}\sum_{\tau\in T_B}\int_{\tau} \frac{h_\tau^2}{12\mu_L}\|\nabla(P)\|^2\, dv, \quad (27)$$

where h_τ is the diameter of the circumscribed circle to an element τ (T. J. R. Hughes, personal communication, 1998) and T_B is the triangulation of the aggregate. Whereas the linear-linear element as a pure Galerkin method is not convergent, the mixed formulation with the stabilizing term of (27) is stable, convergent, and accurate; this property has been demonstrated for small deformation elasticity of an incompressible isotropic material [*Hughes and Franca*, 1987; *Hughes et al*., 1986], in which case equations are the same as for Stokes flow and for finite deformations [*Klaas et al*., 1999; *Liu et al*., 2000; *Maniatty et al*., 2000]. Element stiffness matrices and right-hand side vectors are given by *Bonet and Wood* [1997] and *Dupin* [1999].

Here $\bar{\theta}_\tau$, the average expansion needed for evaluation of (23), is constant elementwise. Noting $\langle dX_{A_{L_i}}\rangle$ and $\langle dX_{I_{L_i}}\rangle$ as the total increase of active and inert biomass, respectively, during $\Delta t = 12$ min at each node, $\bar{\theta}_\tau$ is computed from the total biomass growth between two aggregate shape updates as

$$\bar{\theta}_{N+1_\tau} = \bar{\theta}_{N_\tau}\left(\frac{\overline{dX}_\tau}{X_m} + 1\right), \quad (28)$$

where

$$\overline{dX}_\tau = \sum_{i\in\tau}\left(\frac{\langle dX_{A_{L_i}}\rangle + \langle dX_{I_{L_i}}\rangle}{3}\right). \quad (29)$$

Note that there are three nodes i per element.

After expansion of the aggregate the individual biomass concentrations at each node are projected backward from the elementwise constant density as this elementwise density after deformation is slightly different from the reference density. Indicating with a prime a value after deformation, i a generic node in the mesh (there are three nodes i per element) and $X_{A_{L^i}}$ the active biomass concentration at this node, the global conservation of mass is written

$$\int_{\Omega_B} X'_A\, dv = \int_{\Omega_B} X_A\, dv \quad (30)$$

or, after discretization,

$$\sum_{\tau\in T_B}\left(\sum_{i\in\tau}\frac{|\tau|}{3}X_{A_{L_i}}\right) = \sum_{\tau'\in T'_B}\left(\sum_{i\in\tau'}\frac{|\tau'|}{3}X'_{A_{L_i}}\right), \quad (31)$$

and permuting the summation,

$$\sum_{i\in\Omega_B}\left(\sum_{\tau\in T_B|i\in\tau}\frac{|\tau|}{3}X_{A_{L_i}}\right) = \sum_{i\in\Omega_B}\left(\sum_{\tau'\in T'_B|i\in\tau'}\frac{|\tau'|}{3}X'_{A_{L_i}}\right). \quad (32)$$

Thus we can express local conservation of mass as conservation of the total mass in the support of each node (the elements that contain that node), which can be written as

$$\forall\, i\in\Omega_B, \qquad \left(\sum_{\tau\in T_B|i\in\tau}\frac{|\tau|}{3}\right)X_{A_{L_i}} = \left(\sum_{\tau'\in T'_B|i\in\tau'}\frac{|\tau'|}{3}\right)X'_{A_{L_i}}, \quad (33)$$

that is,

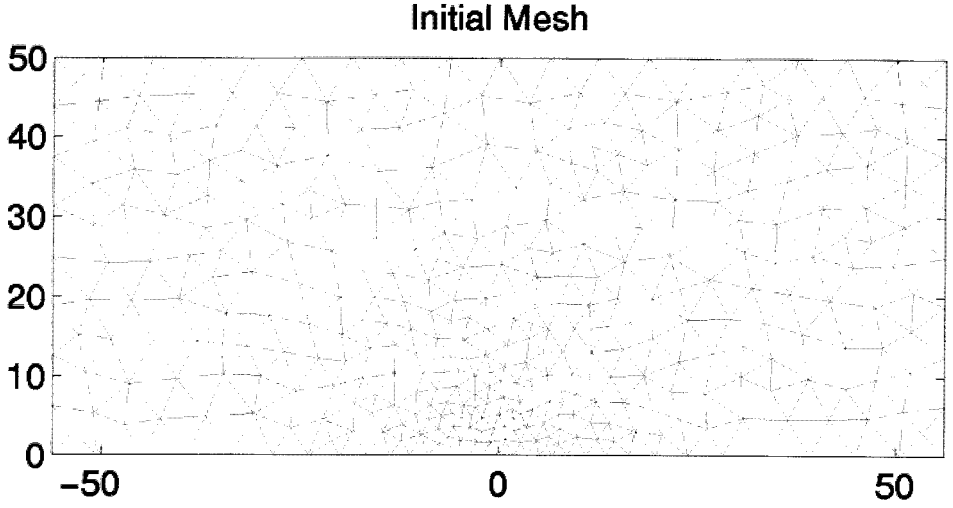

Figure 4. Initial mesh. Dimensions are in micrometers.

$$\forall\, i \in \Omega_B, \qquad X'_{A_{L_i}} = \frac{\left(\sum_{\tau \in T_B | i \in \tau} \frac{|\tau|}{3} \right) X_{A_{L_i}}}{\sum_{\tau' \in T_B | i \in \tau'} \frac{|\tau'|}{3}}. \tag{34}$$

This scheme has been carried out for X_I as well. It can be interpreted as follows: The biomass expansion and deformation increase the size of the elements. However, because of the pseudoincompressibility it shuffles biomass locally among all the elements containing a specific node.

3.5. Mesh Deformation

Instead of remeshing the domain after each aggregate expansion, the mesh of the aggregate is kept deformed. We impose that, by continuity, the mesh of the fluid portion Ω_F deforms in a manner consistent with the aggregate deformation and the pore geometry. The topology of the mesh (i.e., the definition of the elements from the nodes of the mesh) is not changed. Rather, only the individual locations of the nodes are modified. To be consistent with the biomass deformation, the nodes of Ω_F at the aggregate-fluid interface Γ_{B-F} move as they do during the aggregate deformation. To be consistent with the geometry of the pore, the nodes on each other surface (wall Γ_w, inlet Γ_{in}, and outlet Γ_{out}) slide along these surfaces with no frictional resistance. Such method is called arbitrary Lagrangian-Eulerian in modeling of fluid-structure interactions [*Hughes et al*., 1981].

A modified Stokes flow formulation is used and consists in adding to (2) a compression term proportional to the virtual pressure $\tilde{P}$ (i.e., some pressure with no physical meaning), so that (2) becomes

$$\nabla \cdot \mathbf{u} - \gamma \tilde{P} = 0, \tag{35}$$

where $\mathbf{u}$ represented the artificial displacement of the nodes. Formulation for the element matrices and right-hand side vectors is given by *Dupin* [1999], following [*Cao*, 1995]. The same stabilization term used for the Stokes flow problem is added to (35).

This method gradually degrades the mesh quality. Remeshing is performed when the mesh quality has degraded too much, that is, when the ratio

$$\frac{4\sqrt{3}\,|\tau|}{\sum_{i=1}^{3} h_i^2}$$

has become smaller than 0.6 for more than six triangles. When remeshing is performed, we linearly project the values of the variables within the old mesh into the new mesh. The values of the variables at the new nodes (not necessarily coinciding with old nodes) are linearly interpolated from the values within the old triangulation. According to *Jansen et al*. [1992] this method is an optimum trade-off between accuracy and computational cost for unstructured meshes. To compute $\bar{J}$, the elementwise constant Jacobian of the deformation, we store as an additional variable the position that the nodes have within the original mesh at $t = 0$. Those coordinates are linearly interpolated at each remeshing.

4. Results

We present results at time $t = 19.4$ hours of the modeling of an idealized 50 μm wide and 600 μm long pore, seeded with an initial colony 5 μm in radius and subjected to a constant head across of 10^{-3} cm. Electron donor and acceptor supply concentrations are $10K_S$.

Figure 4 shows the initial mesh. The 110 μm long discretized domain is significantly shorter than the full 600 μm long domain. Figure 5 shows the fluid velocity field solution $\mathbf{u}$ of the Stokes problem. As desired, fluid flows around the aggregate because the pseudoviscosity of water in the aggregate is 2000 times higher than normal water viscosity. When the aggregate spans the entire pore and attaches to the opposite wall, flow is forced through the aggregate: The hydraulic conductivity decreases sharply. After 19.4 hours the average velocity is 1.5 m d^{-1}, whereas it equals 2.9 m d^{-1} at $t = 0$.

Plate 1 shows the concentration profiles in the pore of the electron donor (C_D) and the electron acceptor (C_A) as well as the biomass density profiles X_A and X_I before the aggregate expands, normalized to the maximum solids concentration in the aggregate X_m. Maximum growth occurs on the upgradient side of the aggregate, while minimum growth occurs on the wall between the center and the downgradient side of the

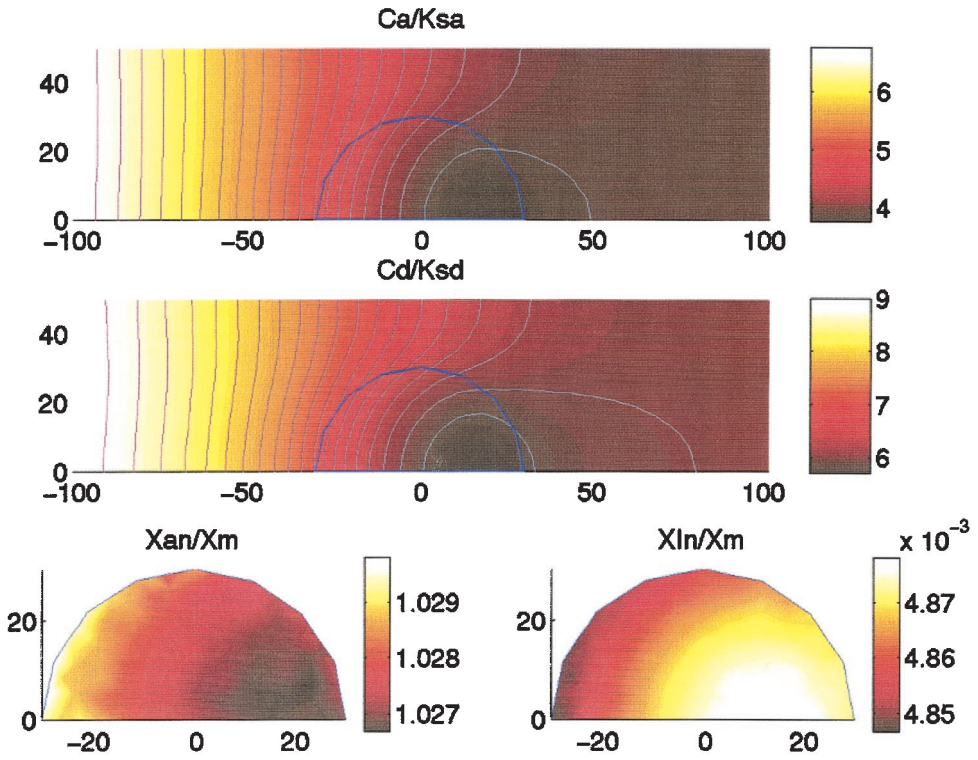

Plate 1. Substrate and biomass concentration profile in the pores. Superposed on the color plots are 20 equally spaced isoconcentration contour lines. Color scales are optimized for contrast and differ for each plot. Distances are in micrometers.

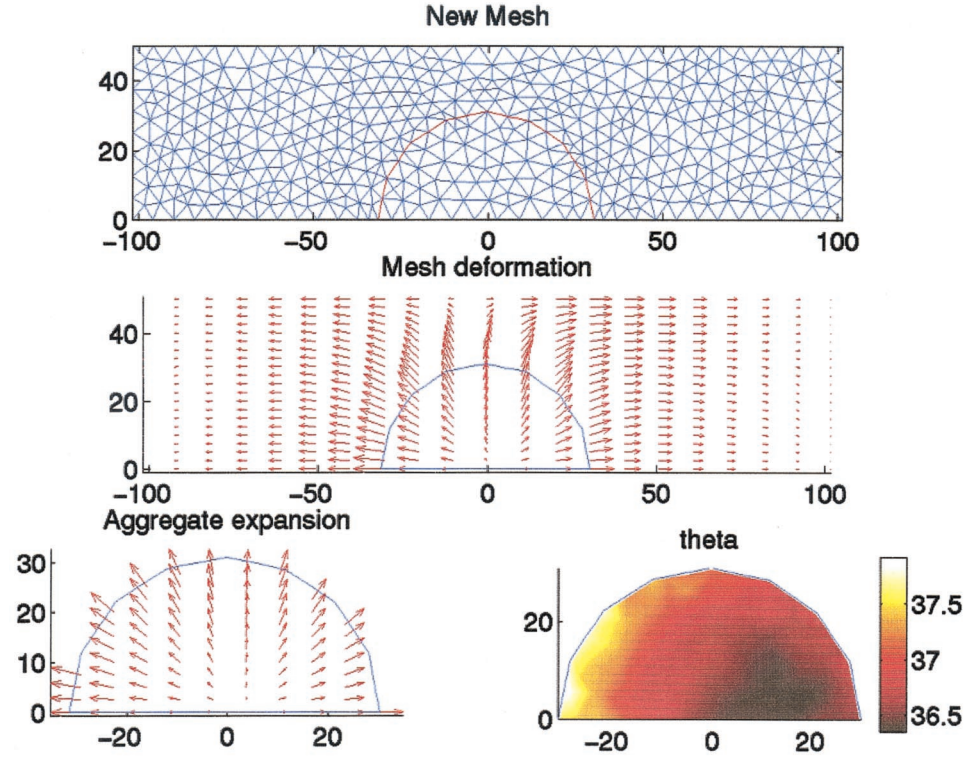

Plate 2. Expansion of the aggregate and deformation of the mesh. Dimensions are in micrometers.

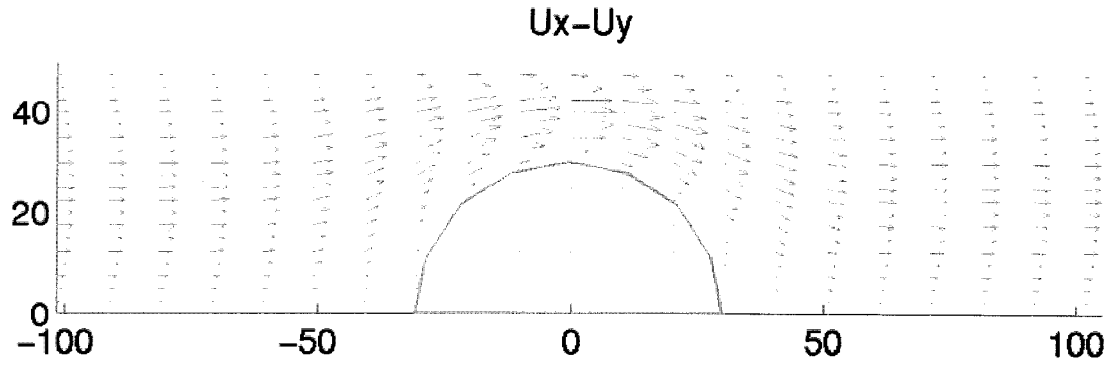

Figure 5. Solution of the Stokes flow in the pore. Dimensions are in micrometers.

aggregate, as expected. However, as long as the aggregate is fully penetrated ($C \gg K_S$), the asymmetry is minor, and errors created by assuming perfect symmetry are small, of the order of a few percent, which is less than the error due to discretization. When the aggregate expands across the entire pore, the electron donor and the electron acceptor become more limited, and thus growth is strongly asymmetric, most of it occurring on the upgradient side of the aggregate. The electron donor concentration at the inlet of the meshed domain is $\sim 7K_S$, which means that 60 μm away from the aggregate, concentration is 70% of the influent concentration. This indicates a "pull" by the aggregate, i.e., an enhancement of transport through steepening of the concentration gradient. Such enhancement of transport exemplifies the difficulty of setting an a priori mass transport coefficient, as is commonly used in biofilm models to represent mass transfer from a mobile phase (bulk fluid) into biomass.

Because the doubling time is ~3 hours and the decay rate is 0.12 day^{-1} (i.e., the decay halftime is ~5.8 days), inert remains X_I represent a very small fraction of the aggregate mass (<0.5% after 19.4 hours).

The effluent electron acceptor and electron donor concentrations equal $4.19K_S$ and $6.13K_S$, respectively. Thus ~60% of the influent electron acceptor is consumed by the aggregate at high flow velocities, ~1.5 m day^{-1}. However, if influent concentration were higher, the amount of electron acceptor and electron donor used would be about the same, because at high concentration Monod kinetics simplifies to zero order reaction, and a smaller percentage of the substrate fed to the channel would be degraded.

For purposes of mass balance verification, biomass $X_m\Omega_B(t_0 + \Delta t)$ and its increase during Δt, $\Delta M_X = X_m[\Omega_B(t_0 + \Delta t) - \Omega_B(t_0)]$, are compared with the mass of electron donor and electron acceptor consumed, $\Delta M_C = U_{\text{ave}}(t_0)[C_{\text{supply}} - C_{\text{effluent}}(t_0 + \Delta t)]\Delta t$, through posttreatment of the saved numerical results. Mass balance (quantified by the correction needed on the effluent concentrations or on the average discharge to satisfy mass balance) is generally satisfied within a few percentage points, which was deemed satisfactory considering numerical inaccuracies from time and spatial discretization. At early times, when the aggregate is small and the mass discharge is high, the decrease in substrate concentration due to consumption ($C_{\text{supply}} - C_{\text{effluent}}$) is comparable to the numerical error on the effluent concentration. At later times, substrate consumption leads to a significant decrease in the substrate concentration at the outlet, and mass balance is much better verified. Furthermore, experimentation with various grid sizes indicated that refining the mesh leads to a better mass balance, even at early times. In the specific case shown in this paper, increasing the model-computed effluent concentration of electron donor and electron acceptor by 1.6% throughout the whole numerical simulation improved performance and was sufficient to yield to values of $\Delta M_X/\Delta M_{C_A}$, $\Delta M_X/\Delta M_{C_D}$, and $\Delta M_{C_A}/\Delta M_{C_D}$ within 1% of their expected values, which are based on integration over the whole aggregate of the sink and source terms F_1-F_4 of (7)–(10).

Plate 2 represents the expansion of the aggregate corresponding to growth from $t = 19.2$ hours to $t = 19.4$ hours and the deformation of the whole mesh. Arrows are about 5 times longer than the computed displacements. Also on Plate 2 is the expansion of the aggregate since $t = 0$, computed as theta = $\bar{J}_t/\bar{J}_{t=0}$. One can again observe the slight asymmetry of growth. The meshed domain extends over a length of 210 μm, instead of 110 μm at the beginning.

Figure 6 shows the outline of the aggregate every 5 hours in a 100 μm wide pore operated with a constant average velocity of 2.9 m d^{-1}. The aggregate is squeezed between the two pore

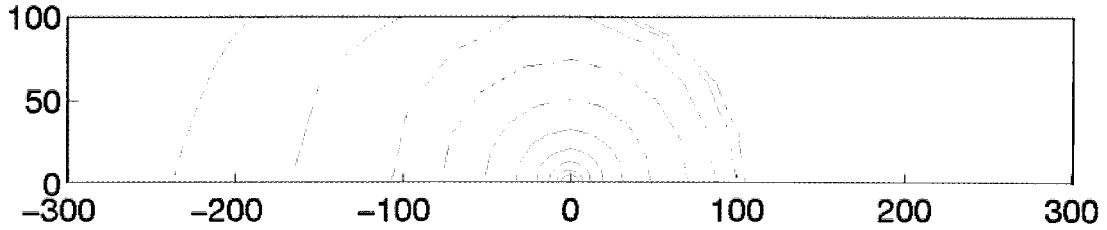

Figure 6. Outline every 5 hours of an aggregate growing in a 100 μm wide pore with a constant average flow velocity of 2.9 m d^{-1}. Dimensions are in micrometers.

walls as it grows. At later times, growth occurs only on the upgradient portion of the aggregate.

5. Discussion

This paper has presented a microscale model of biological growth in an idealized pore. Like other biological growth models, substrate consumption here results in biomass synthesis and biomass expansion. We fully simulate mass transport by solving the Stokes flow problem and the advection-dispersion-reaction equations, without assuming a mass transfer coefficient. Indeed, because the mass transfer coefficient from a fluid into a solid depends on the boundary conditions, especially the sink term in the solid, such mass transfer coefficient cannot be estimated a priori.

A novel feature of this approach is that the expansion of aggregates is proposed to obey material mechanics equations rather than an empirical expansion scheme. Computing biomass expansion from a given increase in the mass of biological matter due to synthesis of new material is not a trivial task. In biofilm models an increase in mass usually translates into a corresponding increase in the thickness of the biological matter. That is, growth occurs in a direction normal to the surface of attachment, and there is generally no movement along the surface (colonization or similar patterns at later times) [*Anderson and McCarty*, 1994; *Atkinson and How*, 1974; *Bouwer and McCarty*, 1985; *Rittmann and McCarty*, 1980, 1981; *Suchomel et al*., 1998]. When representing biomass as microcolonies, that is, patchy biofilms, several empirical options are used to represent biomass increase: increasing the number of colonies whose individual sizes and aspect ratio do not change [*Molz et al*., 1986], increasing the size of a fixed number of microcolonies maintaining their aspect ratio, or a combination of these two approaches. *Picioreanu et al*. [1998a] used a discrete automaton as a means to relate increase in biological mass and biomass expansion. The approach used here, a deterministic approach based on material mechanics, is computationally intensive. It may not be necessary in cases where the biofilm approach or other simple approaches have been shown to be sufficient, especially when substrate consumption in fairly coarse porous media is the only concern. It may, however, be a useful approach when modeling biological clogging in finely grained porous media [*Dupin et al*., this issue].

The particular rheology we have chosen may be open to argument, but it would be fairly straightforward to modify the stress-strain relations as experimental data become available. In particular, biomass material is unlikely to be perfectly hyperelastic, as assumed here, but it may be somehow plastic. Here the description of biomass (as being similar to thermo-hyperelastic rubber) leads to reversible deformations; that is, there is a "back to the original" state deformation (i.e., for the analogy to rubber, cooling of the rubber to restore its original volume and stress relaxation to restore its original shape). However, biomass growth is certainly not a reversible process. First, new cells do not completely vanish when decaying but remain as inert solids. Second, newly formed biomass material may not completely inherit the deformed state of the "parent" material: Some extracellular polymers already existing before formation of daughter cells may keep their deformed states during expansion of new cells, whereas newly formed extracellular polymers are likely to be synthesized "stress free" or at least with different initial stresses. A two-dimensional analog that illustrates this concept is a piece of sheet metal being continuously deformed (say, slowly bent into a broad curve). Imagine that the bending motion is temporarily halted so that one side of the sheet metal can be painted. If the bending motion is then resumed, the paint layer will suffer only the deformation incurred after it was applied and not the entire deformation suffered by the adjacent metal. Nevertheless, in the present context this inaccuracy is unlikely to substantially affect the overall conclusions drawn from the model because of the minor deformation stresses within the aggregates resulting from the chosen boundary conditions.

The particular boundary conditions for the aggregate deformation are also debatable. However, comparison of observed aggregate growth (Figure 1) and simulated aggregate growth (Plate 2) indicates that our assumptions result in reasonable behavior. Additionally, because stresses within the aggregate are computed, detachment by fracture of the aggregate along the lines of maximum stress can be incorporated into the model to allow for more realistic simulations. This stress-computed detachment could provide a mechanistic link between fluid flow, growth, and detachment of pieces of an aggregate. Similarly, attachment or sloughing off of a whole aggregate could be determined by comparing the required adhesion for an aggregate to remain on a surface (given the stresses stemming from fluid flow and the particular displacement boundary conditions of that aggregate along a surface) and, for example, a given bonding strength that may incorporate "curing" or "aging" of the polymers that serve to attach biological matter to solid surfaces or other materials.

This model does not take into account cell-cell signaling that could also affect growth of the aggregate. Other neglected factors are changes in growth rates in cells that are under high stress or extreme low stress. These factors can be incorporated into this model as data become available, because stress is computed throughout the aggregate.

The deterministic approach detailed in this paper will lead to biological masses with a "smooth" outer surface. This is because the outer cells are not free to grow out in the bulk fluid in a random manner but grow in such a manner that the potential energy of the whole aggregate is kept to a minimum. However, there is little ground for a new cell on the outer surface to be constrained in the position it will occupy, except because of viscous forces exerted by the bulk fluid passing by (in the absence of cell-cell signaling). An hybrid model that would incorporate material mechanics to constrain the deformation of the aggregate due to the synthesis of material inside the biological mass and some random model that would allow freedom to the outer cells may better reproduce reality, that is, introduce some roughness [*Gibbs and Bishop*, 1995; *Hermanowicz et al*., 1995]. Such a model may require a discretization of the material with elements whose size approaches that of a cell. Then, the continuum medium approach may no longer be valid, because cells and extracellular polymers have different mechanical properties. Further, diffusion of solutes at this submicronic scale within biological matter will not be homogeneous, that is, cannot be represented by a Fickian law. Other hypotheses, experimental results, and mathematical developments would then be needed.

Finally, the impact of biological matter on flow is modeled by artificially increasing the water viscosity within the aggregate. Another approach could consist in modeling biological mass as a poroelastic material, whereby the action of water on the aggregate would translate into body forces, rather than forces on the outer surface of the aggregates. Depending on

the particular conditions (flow, boundary conditions, etc), this may lead to differences in the result of the simulations. This has not been evaluated in this paper as the action of fluid flow on the shape of the aggregate has been neglected. The formulation (in particular (20)) allows the incorporation of such body forces.

In this paper, only one aggregate is supposed to grow in a given pore and remain there. Future developments could include, besides the implementation of the intricate concepts listed above, simpler modifications such as attachment of several aggregates in a single pore, detachment of pieces (or sloughing off of the whole) of such aggregates, and the simulations of the migration of such aggregates in the porous media.

The method presented in this paper allows simulation of aggregate growth throughout entire pore volumes. This model for aggregate growth at the scale of a pore can then be incorporated into a network model to simulate biological growth and clogging of porous media [*Dupin et al*., this issue]. Comparisons can then be made with biofilm-based models.

Notation

b decay coefficient.
C, C_A, C_D generic concentration, concentration of electron acceptor (oxygen), and electron donor (phenol), respectively.
$\mathbf{C}$, $\hat{\mathbf{C}}$ right Cauchy-Green deformation tensor, deviatoric part of $\mathbf{C}$.
COD chemical oxygen demand of phenol.
d_c decay oxygen demand.
$\langle dX_{A_{L_i}} \rangle$, $\langle dX_{I_{L_i}} \rangle$ total increase of active and inert biomass, respectively, during $\Delta t = 12$ min at each node.
D_a, D_d aqueous diffusion coefficient of oxygen and phenol, respectively.
D_{fa}, D_{fd} diffusion coefficient in an aggregate of oxygen and phenol, respectively.
D_{eff}, $D_{A_{\text{eff}}}$, $D_{D_{\text{eff}}}$ effective diffusion coefficient (of electron acceptor and electron donor, respectively).
$\mathbf{f}_0$ body forces.
F oxygen to phenol utilization ratio.
$\mathbf{F}$ deformation gradient.
F_1, F_2, F_3, F_4 production rates for electron acceptor, electron donor, active biomass, and inert remains, respectively.
f_d degradable biomass fraction.
g gravity.
J, $\bar{J}$ Jacobian of $\mathbf{F}$, elementwise Jacobian.
k maximum utilization rate.
K_S, K_{sA}, K_{sD} saturation constant (of electron acceptor and electron donor, respectively).
l unit length.
L_{pore} pore length.
P Lagrange multiplier that can be identified to the aggregate internal pressure.
$\tilde{P}$ mesh virtual pressure.
Pe_x Peclet number.
t time.
$\mathbf{t}_0$ traction forces on the actual boundary.
T_B temperature aggregate triangulation.
$R_{\text{aggregate}}$ aggregate thickness.
$\mathbf{u} = (u_x, u_y)$ velocity field.
U compression energy for the aggregate.
W_{pore} pore width.
$\mathbf{X}$ original (material) coordinate of a point.
X_A, $X_{A_{L_i}}$ active biomass concentration at a generic point and at a node, respectively.
X_I inert remains concentration.
Y yield coefficient.
α volumetric thermal expansion coefficient.
γ mesh compressibility.
Γ_{in}, Γ_{out}, Γ_{B-F}, Γ_{B-w} inlet, outlet, interface aggregate fluid, aggregate wall, respectively.
δp arbitrary change in P (for linearization).
Δt time step for aggregate expansion.
θ, $\bar{\theta}_\tau$ total expansion since $t = 0$ of a point in the aggregate and an element, respectively.
κ isothermal bulk modulus.
λ ratio of pseudoviscosity of water in an aggregate to the normal viscosity of water.
μ_L lame coefficient.
$\nu_{S_{\text{eff}}}$, ν_{water} effective kinematic viscosity and kinematic viscosity of water.
$\Pi_L(\boldsymbol{\phi})$ total potential energy of the biomass aggregate.
τ element.
φ hydraulic head.
$\boldsymbol{\phi}(\mathbf{X}, t)$ position of the biomass body at time t.
Ψ hyperelastic potential.
Ω, Ω_B, Ω_{B_0}, Ω_F full domain, aggregate domain, initial aggregate domain, and fluid domain, respectively.

Acknowledgments. We want to thank Jun Cao for valuable discussions that jump started our work using the finite elements methodology. Thomas Hughes provided helpful suggestions for the material mechanics problem. Jeff Cunningham and Olaf Cirpka helped improve this manuscript by critically reviewing it. This research was supported in part by the Office of Research and Development, U.S. Environmental Protection Agency, through the Western Region Hazardous Substance Research Center under agreement R-815738, and in part by Elf Aquitaine, Inc. Additional support was provided by NSF under grant 9523922. This article has not been reviewed by those organizations, and thus no official endorsement should be inferred.

References

Anderson, J. E., Effect of chlorinated ethene biodegradation on growth rates of methanotrophic bacteria in biofilms and mixed cultures, Ph.D. thesis, Stanford Univ., Stanford, Calif., 1996.

Anderson, J. E., and P. L. McCarty, Model for treatment of trichloroethylene by methanotrophic biofilms, *J. Environ. Eng*., *120*(2), 379–400, 1994.

Atkinson, B., and S. How, The overall rate of substrate uptake (reaction) by microbial films, Part II, Effect of concentration and thickness with mixed microbial films, *Trans. Inst. Chem. Eng*., *52*, 260–268, 1974.

Baveye, P., and A. Valocchi, An evaluation of mathematical models of the transport of biologically reacting solutes in saturated soils and aquifers, *Water Resour. Res*., *25*(6), 1413–1419, 1989.

Berkowitz, B., and R. P. Ewing, Percolation theory and network modeling applications in soil physics, *Surv. Geophys*., *19*(1), 23–72, 1998.

Bonet, J., and R. D. Wood, *Nonlinear Continuum Mechanics for Finite Element Analysis*, 248 pp., Cambridge Univ. Press, New York, 1997.

Bouwer, E. J., and P. L. McCarty, Utilization rates of trace halogenated organic compounds in acetate-grown biofilms, *Biotechnol. Bioeng.*, *27*(11), 1564–1571, 1985.

Cao, J., Estimations d'erreurs a priori et techniques d'adaptation en éléments finis pour la simulation numérique d'écoulements de fluides visqueux, Thèse de 3ème cycle, Univ. Pierre et Marie Curie (Paris VI), Paris, France, 1995.

Cao, J., and P. Kitanidis, An algorithm for solving reactive advection-dispersion problems, in *Environmental Fluid Mechanics and Hydrology*, report, Dep. of Civ. and Environ. Eng., Stanford Univ., Stanford, Calif., 1998.

Chen, B., A. Cunningham, R. Ewing, R. Peralta, and E. Visser, Two-dimensional modeling of microscale transport and biotransformation in porous media, *Numer. Methods Partial Differ. Equations*, *10*(1), 65–83, 1994.

Chen, B., A. Cunningham, and E. Visser, Numerical simulation of biofilm growth in porous media at the microscale, in *11th International Conference on Computational Methods in Water Resources*, pp. 69–76, Comput. Mech., Billerica, Mass., 1996a.

Chen, J.-S., C. Pan, C.-T. Wu, and W. K. Liu, Reproducing kernel particle methods for large deformation analysis of non-linear structures, *Comput. Methods Appl. Mech. Eng.*, *139*(1–4), 195–227, 1996b.

Clement, T. P., B. S. Hooker, and R. S. Skeen, Macroscopic models for predicting changes in saturated porous media properties caused by microbial growth, *Ground Water*, *34*(5), 934–942, 1996.

Cunningham, A. B., W. G. Characklis, F. Abedeen, and D. Crawford, Influence of biofilm accumulation on porous media hydrodynamics, *Environ. Sci. Technol.*, *25*(7), 1305–1311, 1991.

Cunningham, A. B., E. Visser, Z. Lewandowski, and M. Abrahamson, Evaluation of a coupled mass transport-biofilm process model using dissolved oxygen microsensors, *Water Sci. Technol.*, *32*(8), 107–114, 1995.

Dupin, H. J., Biological and hydrodynamic factors affecting aquifer clogging during in-situ bioremediation, Ph.D. thesis, Stanford Univ., Stanford, Calif., 1999.

Dupin, H., and P. McCarty, Mesoscale and microscale observations of biological growth in a silicon pore imaging element, *Environ. Sci. Technol.*, *33*(8), 1230–1236, 1999.

Dupin, H., and P. L. McCarty, Impact of colony morphologies and disinfection on biological clogging in porous media, *Environ. Sci. Technol.*, *34*(8), 1513–1520, 2000.

Dupin, H., P. Kitanidis, and P. McCarty, Simulations of two-dimensional modeling of biomass aggregate growth in network models, *Water Resour. Res.,* this issue.

Fatt, I., The network model of porous media, I, Capillary pressure characteristics, *Trans. Am. Inst. Min. Metall. Pet. Eng.*, *207*, 144–159, 1956a.

Fatt, I., The network model of porous media, II, Dynamic properties of a single size tube network, *Trans. Am. Inst. Min. Metall. Pet. Eng.*, *207*, 160–163, 1956b.

Fatt, I., The network model of porous media, III, Dynamic properties of networks with tube radius distribution, *Trans. Am. Inst. Min. Metall. Pet. Eng.*, *207*, 164–181, 1956c.

Gibbs, J. T., and P. L. Bishop, Method for describing biofilm surface roughness using geostatistical techniques, *Water Sci. Technol.*, *32*(8), 91–98, 1995.

Hayduk, W., and H. Laudie, Prediction of diffusion coefficients for nonelectrolyte in dilute aqueous solutions, *AIChE J.*, *20*(3), 611–615, 1974.

Hermanowicz, S. W., U. Schindler, and P. Wilderer, Fractal structure of biofilms: New tools for investigation of morphology, *Water Sci. Technol.*, *32*(8), 99–105, 1995.

Hughes, T. J. R., and L. P. Franca, New finite element formulation for computational fluid dynamics, VII, The stokes problem with various well-posed boundary conditions: Symmetric formulations that converge for all velocity/pressure spaces, *Comput. Methods Appl. Mech. Eng.*, *65*, 85–96, 1987.

Hughes, T. J. R., W. K. Liu, and T. K. Zimmermann, Lagrangian-Eulerian finite element formulation for incompressible viscous flows, *Comput. Methods Appl. Mech. Eng.*, *29*, 329–349, 1981.

Hughes, T. J. R., L. P. Franca, and M. Balestra, New finite element formulation for computational fluid dynamics, V, Circumventing the Babuska-Brezzi condition: A stable Petrov-Galerkin formulation of the Stokes problem accommodating equal-order interpolations, *Comput. Methods Appl. Mech. Eng.*, *59*, 85–99, 1986.

Jansen, K., F. Shakib, and T. Hughes, Fast projection algorithm for unstructured meshes, in *Computational Nonlinear Mechanics in Aerospace Engineering*, edited by S. N. Atluri, pp. 175–204, Am. Inst. of Aeronaut. and Astronaut., Reston, Va., 1992.

Klaas, O., A. Maniatty, and M. S. Shephard, A stabilized finite element method for finite elasticity, *Comput. Methods Appl. Mech. Eng.*, *180*, 65–79, 1999.

Lide, D. (Ed.), *CRC Handbook of Chemistry and Physics*, CRC Press, Boca Raton, Fla., 1991.

Liu, Y., A. M. Maniatty, O. Klaas, and M. S. Shephard, A stabilized mixed FEM for viscoplastic flow analysis, in *IMECE 2000*, *MED*, edited by R. J. Forness, pp. 761–767, Am. Soc. of Mech. Eng., New York, 2000.

Maniatty, A. M., Y. Liu, O. Klaas, and M. S. Shephard, Higher order stabilized FEM for modeling finite deformations, in *Proceedings of Plasticity 2000: Plastic and Viscoplastic Response of Materials and Metal Forming*, edited by A. Kahn, H. Zhang, and Y. Yuan, pp. 83–85, Neat Press, Fulton, Md., 2000.

McCarty, P. L., M. N. Goltz, G. D. Hopkins, M. E. Dolan, J. P. Allan, B. T. Kawakami, and T. J. Carrothers, Full-scale evaluation of in situ cometabolic degradation of trichloroethylene in groundwater through toluene injection, *Environ. Sci. Technol.*, *32*(1), 88–100, 1998.

Molz, F. J., M. A. Widdowson, and L. D. Benefield, Simulation of microbial growth dynamics coupled to nutrient and oxygen transport in porous media, *Water Resour. Res.*, *22*(8), 1207–1216, 1986.

Montgomery, J. H., *Groundwater Chemicals Desk Reference*, 1345 pp., CRC Press, Boca Raton, Fla., 1996.

Nicholson, D. W., and B. Lin, Theory of thermohyperelasticity for near-incompressible elastomers, *Acta Mech.*, *116*(1–4), 15–28, 1996.

Paulsen, J. E., E. Oppen, and R. Bakke, Biofilm morphology in porous media, a study with microscopic and image techniques, *Water Sci. Technol.*, *36*(1), 1–9, 1997.

Picioreanu, C., M. C. M. van Loosdrecht, and J. J. Heijnen, Mathematical modeling of biofilm structure with a hybrid differential-discrete cellular automaton approach, *Biotechnol. Bioeng.*, *58*(1), 101–116, 1998a.

Picioreanu, C., M. C. M. van Loosdrecht, and J. J. Heijnen, New combined differential-discrete cellular automaton approach for biofilm modeling: Application for growth in gel beads, *Biotechnol. Bioeng.*, *57*(6), 718–731, 1998b.

Rittmann, B. E., The significance of biofilms in porous media, *Water Resour. Res.*, *29*(7), 2195–2198, 1993.

Rittmann, B. E., and P. L. McCarty, Model of steady-state-biofilm kinetics, *Biotechnol. Bioeng.*, *22*(11), 2343–2358, 1980.

Rittmann, B. E., and P. L. McCarty, Substrate flux into biofilms of any thickness, *J. Environ. Eng. Div. Am. Soc. Civ. Eng.*, *107*(4), 831–849, 1981.

Semprini, L., and P. L. McCarty, Comparison between model simulations and field results for in-situ biorestoration of chlorinated aliphatics, Part 1, Biostimulation of methanotrophic bacteria, *Ground Water*, *29*(3), 365–374, 1991.

Shurtliff, M. M., G. F. Parkin, L. J. Weathers, and D. T. Gibson, Biotransformation of trichloroethylene by a phenol-induced mixed culture, *J. Environ. Eng.*, *122*(7), 581–589, 1996.

Suchomel, B. J., B. M. Chen, and M. B. Allen III, Network model of flow, transport and biofilm effects in porous media, *Transp. Porous Media*, *30*(1), 1–23, 1998.

Taylor, S. W., and P. R. Jaffe, Biofilm growth and the related changes in the physical properties of a porous medium, 1, Experimental investigation, *Water Resour. Res.*, *26*(9), 2153–2159, 1990a.

Taylor, S. W., and P. R. Jaffe, Substrate and biomass transport in a porous medium, *Water Resour. Res.*, *26*(9), 2181–2194, 1990b.

Taylor, S. W., and P. R. Jaffe, Enhanced in-situ biodegradation and aquifer permeability reduction, *J. Environ. Eng.*, *117*(1), 25–46, 1991.

Taylor, S. W., P. C. D. Milly, and P. R. Jaffe, Biofilm growth and the related changes in the physical properties of a porous medium, 2, Permeability, *Water Resour. Res.*, *26*(9), 2161–2169, 1990.

Vandevivere, P., and P. Baveye, Effect of bacterial extracellular polymers on the saturated hydraulic conductivity of sand columns, *Appl. Environ. Microbiol.*, *58*(5), 1690–1698, 1992a.

Vandevivere, P., and P. Baveye, Saturated hydraulic conductivity reduction caused by aerobic bacteria in sand columns, *Soil Sci. Soc. Am. J.*, *56*(1), 1–13, 1992b.

Vandevivere, P., P. Baveye, D. Sanchez de Lozada, and P. DeLeo, Microbial clogging of saturated soils and aquifer materials: Evaluation of mathematical models, *Water Resour. Res*., *31*(9), 2173–2180, 1995.

Williamson, K., and P. L. McCarty, A model of substrate utilization by bacterial films, *J. Water Pollut. Control Fed*., *48*(1), 9–24, 1976.

H. J. Dupin, Geosciences Department, Exploration-Production Division, Gaz de France, 361 Avenue du Président Wilson BP 33, 93211 Saint-Denis-La-Plaine Cedex, France. (hubert.dupin@gazdefrance.com)

P. K. Kitanidis and P. L. McCarty, Department of Civil Engineering, Stanford University, Panama Mall and Samuel Morris Way, Stanford, CA 94305-4020. (kitanidis@ce.stanford.edu; mccarty@cive.stanford.edu)

(Received April 10, 2000; revised March 21, 2001; accepted June 20, 2001.)